Simulation of Thermomechanical Behavior Subjected to Induction Hardening

Qingzhe Liu, Thomas Petzold, Dawid Nadolski, and Roland Pulch

Abstract Induction hardening is one of the most important heat treatments of steel components. This paper presents a mathematical and numerical model developed for a coupled problem of Maxwell's equations describing the electromagnetic fields, the balance of momentum which determines internal stresses and deformations resulting from thermoelasticity and phase transformation induced plasticity, a rate law to determine the distribution of different phases and the heat equation to determine the temperature distribution in the workpiece. The equations are solved using a finite element method. A good agreement between the simulation results and experiment performed to determine the deformation is observed. In addition, the distribution of residual stresses after the heat treatment is well predicted.

1 Introduction

For many applications in mechanical engineering, especially in automotive industry, there is a growing demand in components made of steel sheets. Therefore, to improve the quality of boundary layers of these sheets is a significant task since one must carefully control the process precisely in order not to harden the complete sheet which may lead to undesirable fatigue effects.

Surface hardening is a well known method for enhancing mechanical properties of steel components. The aim of this heat treatment is to increase the hardness of the boundary layers of components made from steel by rapid heating and subsequent quenching. The reason why the hardness increases relies on a change

Q. Liu (✉) • R. Pulch
Institut für Mathematik und Informatik, Ernst Moritz Arndt Universität Greifswald, 17487 Greifswald, Germany
e-mail: liuq@uni-greifswald.de; pulchr@uni-greifswald.de

T. Petzold
Weierstraß-Institut, Mohrenstr. 39, 10117 Berlin, Germany
e-mail: Thomas.Petzold@wias-berlin.de

D. Nadolski
Stiftung Institut für Werkstofftechnik IWT, Badgasteiner Str. 3, 28359 Bremen, Germany
e-mail: nadolski@iwt-bremen.de

A. Bartel et al. (eds.), *Scientific Computing in Electrical Engineering*, Mathematics in Industry 23, DOI 10.1007/978-3-319-30399-4_14

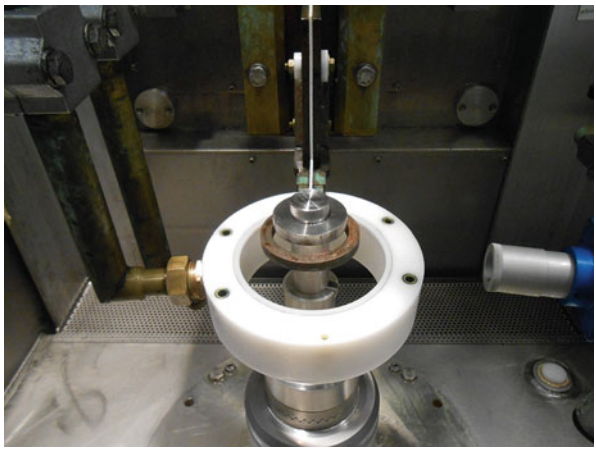

Fig. 1 Induction hardening of a disc (by Stiftung Institut für Werkstofftechnik IWT, Bremen)

in the microstructure of the workpiece during the surface hardening which produces the desired hardening effect.

Depending on heat sources there are different surface hardening procedures. The most import ones are flame hardening, laser hardening and induction hardening. In comparison to flame and laser, induction hardening is advantageous with regard to energy consumption because of the Joule effect resulting from eddy currents.

Figure 1 shows such an experimental set up which consists of an induction coil (inductor), an alternating current power supply, a cooling apparatus and the workpiece (in this experimental set up a disc made from steel) itself as basic components. During the heating stage of this process the inductor is connected to the power supply, the flow of the alternating current through the induction coil induces eddy currents inside the workpiece that lead to increase in temperature due to the Joule effect. Then the current is switched off and the workpiece is quenched by cooling liquid which leads to the desired hardening effect on the boundary layer of the workpiece.

A mathematical model for induction surface hardening accounts for the electromagnetic effects as well as for the thermomechanical behavior and the phase transitions that are caused by enormous changes in temperature during the heat treatment.

The paper is organized as follows. In Sect. 2 we give a brief survey of the complete mathematical model of induction hardening which has been investigated intensively in [2]. Section 3 is devoted to the numerical discretization of the problem. Here a finite element method is applied to solve the system of partial differential equations. The aspect arising from different time scales which needs to be considered in the simulation is addressed. Section 4 focuses on the simulation results of the coupled problem of electromagnetics and thermomechanics in the process of inductive heating for discoid samples made of steel 42CrMo4 (AISI 4140). In comparison to [7] in which only the quenching process has been considered we implement the full procedure, i.e., the induction heating and following

quenching process. Especially we present numerical results of mechanical effects like the residual stress distribution as well as thermally induced distortions where the TRIP (transformation induced plasticity) was involved since this effect is significant in the induction hardening (cf. [6]). From the simulation results a good agreement with experiments according to the deformation is observed and the distribution of residual stresses after the heat treatment is well predicted. Further numerical results of gears samples made of the material AISI 4140 including the determination of the most important properties of the parts for industrial practice, e.g. hardness pattern, residual stresses and distortion have been presented in [3]. The paper ends with a short conclusion and an outlook.

2 The Mathematical Model

For the complete process of heating and cooling we consider the model components corresponding to the electromagnetic field, the temperature evolution, the phase transformations as well as the mechanical deformations and stresses. It accounts for a coupled problem of Maxwell's equations describing the electromagnetic fields, the balance of momentum which determines internal stresses and deformations caused by thermoelasticity and TRIP and the heat equation describing the evolution of temperature distribution in the workpiece. Figure 2 depicts the interrelations among these physical model components. To model the coupled problem of electromagnetics and thermomechanics we first define spatial computational domains. Let $G \subset \mathbb{R}^3$ be a domain which surrounds the inductor Ω and the workpiece Σ.

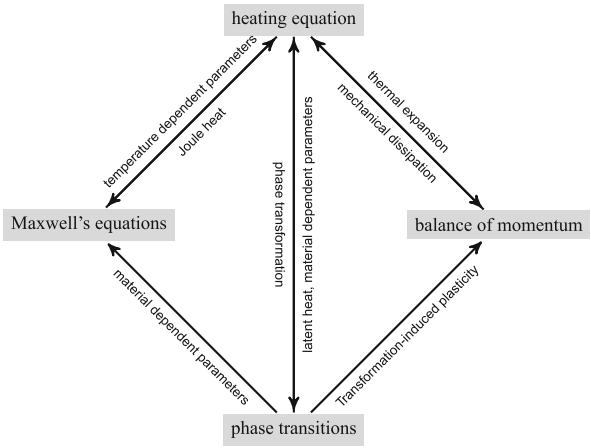

Fig. 2 Mathematical subproblems for induction hardening and their interplays

The electromagnetic effects in G are described by Maxwell's equations that consist of a system of partial differential equations with respect to the electric field $\mathbf{E}$, the magnetic induction $\mathbf{B}$, the magnetic field $\mathbf{H}$ and electric displacement field $\mathbf{D}$, i.e.:

$$\begin{aligned} \operatorname{curl} \mathbf{E} &= -\partial_t \mathbf{B} \\ \operatorname{div} \mathbf{B} &= 0 \\ \operatorname{curl} \mathbf{H} &= \mathbf{J} + \partial_t \mathbf{D} \\ \operatorname{div} \mathbf{D} &= \varsigma \end{aligned} \tag{1}$$

where $\mathbf{J}$ denotes the current density and ς the charge density. In addition Ohm's law yields

$$\mathbf{J} = \gamma \mathbf{E}$$

where γ is the electric conductivity and by constitutive laws we obtain

$$\mathbf{D} = \varepsilon \mathbf{E}, \quad \mathbf{B} = \mu \mathbf{H}$$

with material dependent electrical permittivity ε and magnetic permeability μ. We introduce the magnetic vector potential $\mathbf{A}$ such that

$$\mathbf{B} = \operatorname{curl} \mathbf{A},$$

and impose the Coulomb gauge

$$\operatorname{div} \mathbf{A} = 0.$$

Then following [2] we employ the vector potential formulation of Maxwell's equations which has been derived based on Helmholtz decomposition. More details can be found in [3].

With regard to phases, at the beginning of the heating process the workpiece consists of a mixture of ferrite, pearlite, and bainite. At the end of the heating process the outer layers of the workpiece have been transformed to austenite. The phase evolution of austenite is described along the ideas given in [9]. Then upon rapid quenching the austenite fraction is transformed to martensite. The rate laws describing phase evolutions during cooling have been presented in [6, 7].

The thermomechanical behavior in the complete process can be modeled by laws of energy balance and balance of momentum (cf. [3]). The coupling interface between temperature and deformation is thermal expansion and backward mechanical dissipation.

In summary, the governing equations of the electromagnetic field, the temperature evolution, the mechanical deformations and stresses as well as the steel phase transformations read as follows:

$$\begin{aligned} \gamma \partial_t \mathbf{A} + \operatorname{curl} \mu^{-1} \operatorname{curl} \mathbf{A} - \mathbf{J}_{\text{src}} &= \mathbf{0}, \quad \text{in } G \\ \rho c_\varepsilon \partial_t \theta - \operatorname{div} k \nabla \theta &= F, \quad \text{in } \Sigma \\ -\operatorname{div} \boldsymbol{\sigma} &= \mathbf{0}, \quad \text{in } \Sigma \\ \dot{\mathbf{z}} - \mathbf{f}(\mathbf{z}, \theta, t) &= \mathbf{0}, \quad \text{in } \Sigma \\ \dot{\boldsymbol{\varepsilon}}^{\text{trip}} - g(\boldsymbol{\sigma}, \theta, \mathbf{z}, \dot{\mathbf{z}}) &= 0, \quad \text{in } \Sigma \end{aligned} \tag{2}$$

where the variables $(\mathbf{A}, \theta, \boldsymbol{\sigma}, \mathbf{z}, \boldsymbol{\varepsilon}^{\text{trip}})$ denote the magnetic vector potential, the temperature, the stress tensor, phase fraction and phase transformation induced plasticity (TRIP) strain, respectively. For isotropic materials the stress tensor $\boldsymbol{\sigma}$ which is a matrix valued function admits a expression in terms of the displacement $\mathbf{u}$ (cf. [3, 7]). Here the divergence of the tensor $\boldsymbol{\sigma}$ is a vector field defined by the divergence for each row of the tensor matrix. The material dependent parameters $(\gamma, \mu, \rho, c_\varepsilon, k)$ denote electrical conductivity, magnetic permeability, density of the workpiece, specific heat and heat conductivity. $\mathbf{J}_{\text{src}}$ denotes the source current density satisfying $-\operatorname{div} \mathbf{J}_{\text{src}} = 0$, F summarizes the source term caused by Joule heat, mechanical dissipation and latent heat due to phase transitions. Here the vector potential formulation of Maxwell's equations is taken into account, the heating equation has been derived from energy balance, the deformation equation is based on balance of momentum, the rate of change of phase fractions $\mathbf{f}$ results from the Johnson-Mehl-Avrami equation (cf. [8]) and Schröder's approach, see e.g. [5]. The equation describing the evolution of TRIP $\boldsymbol{\varepsilon}^{\text{trip}}$ is derived from the Franitza-Mitter-Leblond proposal (cf. [1]).

All material parameters depend strongly upon the temperature θ and phase distribution $\mathbf{z}$. The intermediate coupling interface of heating equation [the second equation of (2)] and mechanical equation [the third equation of (2)] comprises the thermal strain, denoted by $\boldsymbol{\varepsilon}^{\text{th}}$ which corresponds to the mechanical strain resulting from temperature change and can be expressed by thermal expansion coefficient and the mechanical dissipation, i.e.,

$$\sigma : (\dot{\boldsymbol{\varepsilon}}^{\text{th}} + \dot{\boldsymbol{\varepsilon}}^{\text{trip}})$$

which reactively influences temperature and is involved in the source term of heating equation. Moreover, the term of Joule heat $\gamma |\partial_t \mathbf{A}|^2$ couples electromagnetics and thermomechanics.

3 Numerical Discretization

The workpiece boundary is dissected into a part τ_s which is free from any acting force and a part τ_u where the workpiece is fixed. The method of lines (MOL) is applied for discretization of Eq. (2). The first step is to discretize the partial differential equations with respect to space while keeping the time variable continuous. Here the spatial discretization is achieved by tetrahedral mesh generation.

Using curl-conforming finite elements we introduce the solution space of the vector potential $\mathbf{A}$:

$$\mathbb{H}(\text{curl}, G) = \left\{\mathbf{v} : G \to \mathbb{R}^3 \middle| \mathbf{v}, \text{curl } \mathbf{v} \in [L^2(G)]^3 \text{ and div } \mathbf{v} = 0, \mathbf{v} \times \mathbf{n} = \mathbf{0} \text{ on } \partial G\right\}$$

where $\mathbf{n}$ denotes the normal to the boundary. For the temperature θ and the phase fraction $\mathbf{z}$ we use classical H^1-conforming elements

$$H^1(\Sigma) = \left\{v : \Sigma \to \mathbb{R} \middle| v \in L^2(\Sigma), \nabla v \in [L^2(\Sigma)]^3\right\}$$

while the displacement $\mathbf{u}$ is approximated by vector-valued H^1 elements

$$X^u(\Sigma) = \left\{\mathbf{v} : \Sigma \to \mathbb{R}^3 \middle| \mathbf{v} \in [H^1(\Sigma)]^3, \mathbf{v} \cdot \mathbf{n}|_{\tau_s} = 0, \mathbf{v}|_{\tau_u} = \mathbf{0}\right\}.$$

With these definitions in mind we use a finite element method (FEM) to calculate the unknowns by computing their projections on corresponding finite dimensional subspaces. More precisely, the FE-discretized system (2) is already a system of DAEs for the variables: vector potential, temperature, displacement, phase fractions and TRIP. Concerning discretization in time we solve the heat equation together with the balance of momentum and the ODEs describing the phase transition and TRIP using a 'large' time step Δt resulting from the typical time scale of the heat conduction. To solve the electromagnetic problem in the time interval Δt we use a time step $\delta t \ll \Delta t$ that is related to the source term of the vector potential equation. Here we use a time stepping scheme of order two with time step δt. For more details we refer the reader to [3].

4 Simulation and Experimental Verification

The numerical simulations are carried out on a disc with diameter 47.7 mm made of steel 42CrMo4 (Fig. 3). From symmetry reasons we restrict ourselves to compute only a segment with an angle of $\frac{\pi}{20}$ (cf. Fig. 4). The cross sections are subject to the symmetric boundary conditions, that means the displacement on the symmetric cuts equals zero in normal direction and the normal directional space derivatives of the displacement along the cross sections are zero (cf. [7]). All material parameters

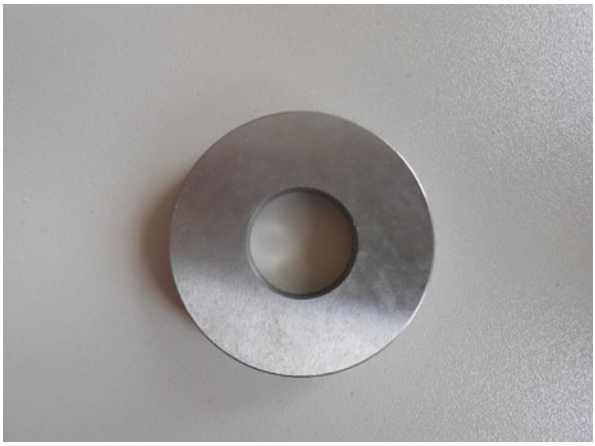

Fig. 3 Disc geometry provided by Stiftung Institut für Werkstofftechnik IWT, Bremen

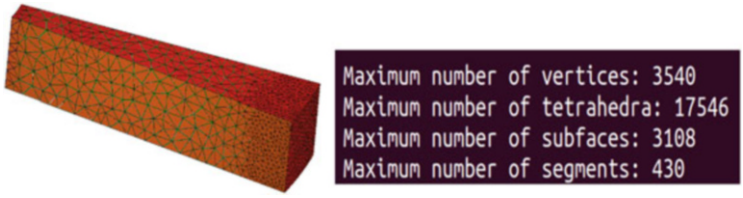

Fig. 4 The reduced computational domain with FE-mesh

associated with 42CrMo4 for the simulations are provided by IWT (Stiftung Institut für Werkstofftechnik, Bremen), and parameters for phase transitions are taken from [4]. All numerical results presented here accompanied with the thermally induced deformation are scaled by 40 to improve their visualizations. According to experimental setting we use a medium frequency 12 kHz with power 100 kW, relative power 63 % and current 575 A, and assume that the surrounding room temperature is 20 °C.

The simulation results of such an induction heating process are visualized. Figure 5 shows progressive temperature values at different heating stages. Owing to the enormous increase in temperature the workpiece suffers from gross distortion caused by thermal expansion during heating. The subsequent cooling process leads to thermal contraction as well as TRIP. Figure 6 shows the corresponding Euclidean norm of the displacement at the beginning of cooling stage and the end of cooling, respectively.

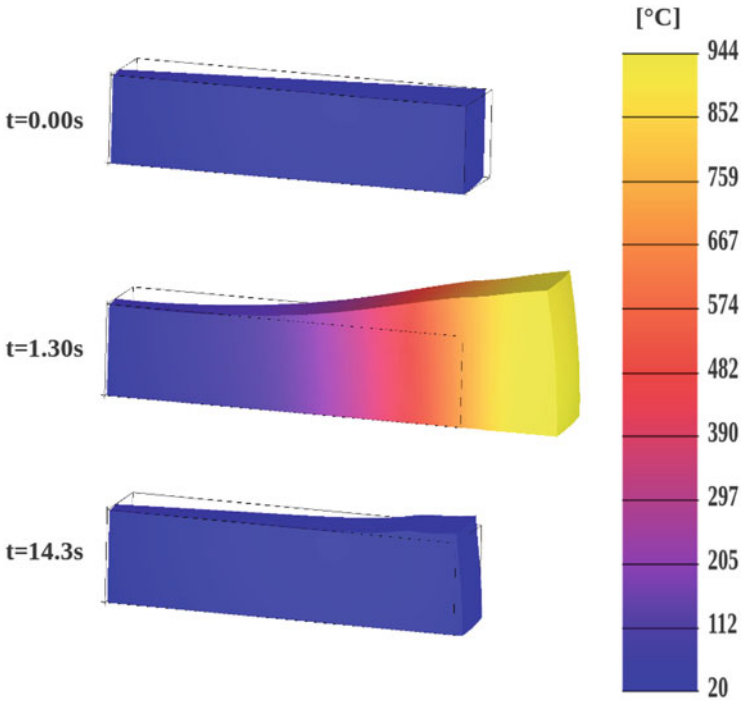

Fig. 5 Temperature evolution at the beginning of heating ($t = 0.00$ s), the beginning of cooling ($t = 1.3$ s), and the end of cooling ($t = 14.3$ s). The deformation is scaled by 40

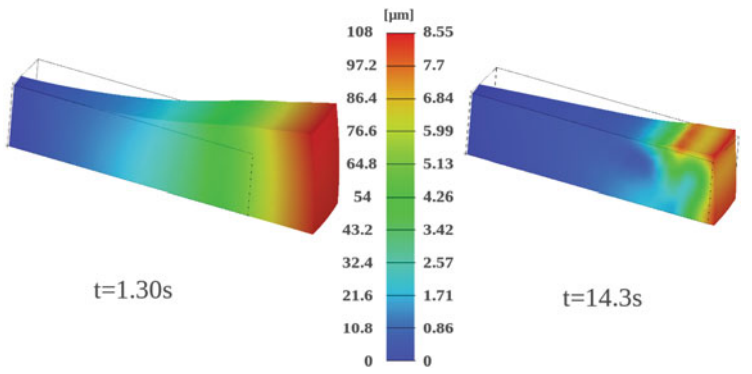

Fig. 6 Euclidean norm of the displacement at the beginning of cooling ($t = 1.3$ s), and the end of cooling ($t = 14.3$ s). The deformation is scaled by 40

Besides, the size change of disc diameter at $t = 14.3$ s (the end of cooling) has been calculated. In Fig. 7 it is obvious that at the boundary layer a maximal stretch of size 9.9 µm is observed. Compared with the original size of the workpiece the dimensional change is relatively slight. A comparison with

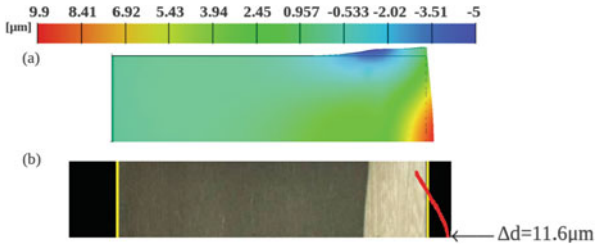

Fig. 7 Size changes of disc diameter; (**a**) simulated results scaled by 40, (**b**) experimental measurements performed by Stiftung Institut für Werkstofftechnik IWT, Bremen; deformations are depicted by the contour which is magnified 200 times

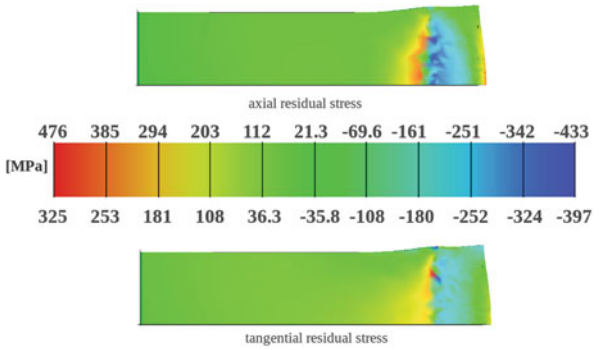

Fig. 8 Axial and tangential residual stresses at the sectional symmetry plane after induction heat treatment

experimentally measured values shows a very good conformance since the absolute error $|11.6 - 9.9|$ µm (cf. Fig. 7) is negligible in industrial practice.

The compressive residual stress distribution in the workpiece which is generated during the phase transformations is considered as one of the most important effects for the enhancement of strength. A numerical result of axial and tangential residual stresses after induction hardening is presented in Fig. 8.

5 Conclusions

In the mathematical treatment of the complete process of induction hardening including heating and quenching stages, a coupled problem of electromagnetics, thermomechanics and phase transitions is taken into account. The numerical simulations based on an FEM are carried out to predict the temperature evolution as well as mechanical behaviors.

Since only simple symmetric workpieces (disc) have been considered in the simulation, the solution with symmetric boundary conditions is not dependent on the angular coordinate and the segment angular openness is not relevant. Consideration of workpieces with complex geometries, helical gears for instance, should be a further application.

In addition, investigations of the effect of uncertain data for the simulation results, optimal control of the inductive heating under consideration of the growth of the high temperature phase austenite remain open problems.

Acknowledgements This research is a part of the project MeFreSim (Modeling, Simulation and Optimization of Multi-Frequency Induction Hardening) funded by Bundesministerium für Bildung und Forschung (BMBF). Furthermore we thank our industrial cooperation partners ZF Friedrichshafen AG and Dr. H. Stiele at EFD Induction GmbH for the technical support.

References

1. Fischer, F.D., Reisner, G., Werner, E., Tanaka, K., Cailletaud, G., Antretter, T.: A new view on transformation induced plasticity (TRIP). Int. J. Plast. **16**, 723–748 (2000)
2. Hömberg, D.: A mathematical model for induction hardening including mechanical effects. Real World Appl. **5**, 55–90 (2004)
3. Hömberg, D., Liu, Q., Urquizo, J.M., Nadolski, D., Petzold, T., Schmidt, A., Schulz, A.: Simulation of multi-frequency-induction-hardening including phase transitions and mechanical effects. Weierstraß-Institut für Angewandte Analysis und Stochastik, Leibniz-Institut im Forschungsverbund Berlin e.V. (2014, preprint). ISSN 2198-5855
4. Mioković, T.: Analyse des Umwandlungsverhaltens bei ein- und mehrfacher Kurzzeithärtung bzw. Laserstrahlhärtung des Stahls 42CrMo4. Dissertation, Universität Karlsruhe, Shaker Verlag Aachen, Band 2005, 25 (2005) ISBN: 3-8322-4689-4, Erschienen: Dezember 2005
5. Schröder, R.: Untersuchung zur Spannungs- und Eigenspannungsausbildung beim Abschrecken von Stahlzylindern. Dissertation, University of Karlsruhe (1985)
6. Urquizo, J.M., Liu, Q., Schmidt, A.: Quenching simulation for the induction hardening process—Thermal and mechanical effects. Berichte aus der Technomathematik, University of Bremen (2013)
7. Urquizo, J.M., Liu, Q., Schmidt, A.: Simulation of quenching involved in induction hardening including mechanical effects. Comput. Mater. Sci. **79**, 639–649 (2013)
8. Visintin, A.: Mathematical models of solid-solid phase transitions in steel. IMA J. Appl. Math. **39**, 143–157 (1987)
9. Wolff, M., Böhm, M., Böttcher, S.: Phase transformations in steel in the multi-phase case - general modelling and parameter identification. Technical Report 07-02, Universität Bremen, Berichte aus der Technomathematik (2007)